

Acoustic metaholograms for encrypted information transmission

Xudong Fan^{1,2,*}, Yifan Zhu,³ Ning Li,¹ Chunsheng Weng,¹ and Badreddine Assouar^{4,†}

¹*National Key Laboratory of Transient Physics, Nanjing University of Science and Technology, Nanjing 210094, China*

²*Key Laboratory of Modern Acoustics, MOE, Nanjing University, Nanjing 210093, China*

³*Jiangsu Key Laboratory for Design and Manufacture of Micro-Nano Biomedical Instruments, School of Mechanical Engineering, Southeast University, Nanjing 211189, China*

⁴*Université de Lorraine, CNRS, Institut Jean Lamour, Nancy F-54000, France*

(Received 5 June 2023; revised 9 August 2023; accepted 5 October 2023; published 18 October 2023)

We report on the theoretical, numerical, and experimental investigation of secure acoustic holography. This secure holography is achieved via an encoded hologram generated by a transducer array decoded by a transmissive acoustic metakey. An unreadable image is received if directly using the encoded hologram, while the desired image can be obtained only with the aid of a decoding metastructure, i.e., a correctly decoding metakey. The proposed metakey consists of a series of unit cells, each of them is composed of a straight channel decorated with several opening panels. By adjusting the opening size of unit cells within the metakey, its transmitted phase profile can be effectively controlled; hence, the desired decoding metakey can be successfully constructed. The patterns of a butterfly, sunglasses, and the letters NJUST are chosen as examples to demonstrate the performance of the secure acoustic holography. Vulnerability tests of the metakey further confirm the safety and reliability of secure acoustic holography. With the advantages of simple design, flexible functionality, and high quality for reconstructed images, our work opens an alternative avenue for acoustic holography and may find applications in secure acoustic communications based on holograms.

DOI: 10.1103/PhysRevApplied.20.044048

I. INTRODUCTION

Acoustic holograms, with the capability for arbitrary sound-field reconstruction, have been broadly studied in the last few years [1–11], offering inspiration for a variety of applications, such as ultrasonic therapy and particle manipulations [12–17]. Holograms are generally realized by either active transducer arrays [3–5] or passive acoustic metamaterials [6–8,18–20], where the phase and/or amplitude response on each hologram pixel are engineered to reconstruct the desired field at a certain spatial location.

For conventional acoustic metaholograms, the phase plate containing phase information is used for field reconstruction [1,2], but the corresponding image quality is, however, barely satisfactory due to the missing amplitude information of holograms. To overcome this limitation, acoustic metaholograms can be realized based on both phase and amplitude information [7,21], so that high-quality images can be reconstructed with no need for optimization. This extraordinary success has broadened the potential applications for acoustic holograms.

At the same time, remarkable progress has been made to achieve holographic images with high efficiency and quality using electromagnetic waves in the terahertz, infrared, and visible regimes [22–34]. Electromagnetic metaholograms can be effectively tuned by controlling either metasurfaces composed of active materials or incident-light sources. For the former, different types of external stimuli are generally applied to active metasurfaces to tune metaholograms, such as electrical [35], thermal [36], chemical [37], and mechanical [38] methods. However, for the latter, a single metasurface can be recycled to produce tunable holographic images by controlling different properties of incident-light sources, for example, the polarization states [39], orbital angular momentum [40], wavelength [41], incident-light angle [42], and coding incident beams [43]. For a more comprehensive review of tunable or dynamic electromagnetic metaholography, see Ref. [44].

The rapid development and great success in electromagnetic metaholograms provide promising potential for information storage and encryption [37,45–49] and inspire acoustic encryption based on holograms. Holographic acoustic encryption, once achieved, will dramatically extend the application scenarios, such as encrypted acoustic information communication, acoustic

*fanxudong@njust.edu.cn

†badreddine.assouar@univ-lorraine.fr

field reconstruction [1,7], acoustic cloaking [50] or illusion [51], architectural acoustics [52], and particle manipulations [4,5,53].

Here, we report on a framework for secure acoustic holograms with the advantages of secure projection, simple design, flexible functionality, and high quality of reconstructed images. For secure acoustic holography, the desired image is obtained only with the aid of an acoustic metakey containing the correct decoding information; otherwise, it produces unreadable images. Here, an acoustic speaker array consisting of 16×16 air-coupled ultrasonic transducers is used to generate the encoded hologram containing both amplitude and enciphered phase information of the transmitted image. Independent modulation of the amplitude and phase for the speaker array provides extreme flexibility for image reconstruction. A different class of unit cells that could effectively modulate transmitted phase shifts of acoustic waves is designed and used to construct the acoustic metakey. The reusable metakey is used to decipher secure information and recover several changeable predesigned images with high fidelity. The patterns of a butterfly, sunglasses, and the letters NJUST are chosen as examples to demonstrate the concept of secure acoustic holography proposed here. Our work provides a conceptual advance for secure acoustic communications based on holograms.

II. PRINCIPLE OF SECURE HOLOGRAPHY

Figures 1(a) and 1(b) show illustrations of secure acoustic holography. A desired holographic pattern is arbitrarily chosen first, for example, a butterfly here, and then the pattern is captured by the acoustic pressure field, denoted by $P(x, y, z)$. To reconstruct this image via an acoustic hologram, the time-reversal method [7] is used to calculate the complex pressure profile on the hologram plane, $p(x, y) = A(x, y) \exp[\phi(x, y)]$, which is discretized into two individual $N \times N$ matrices, i.e., $A_{i,j}$ and $\phi_{i,j}$, with $i, j = 1, 2, \dots, N$. These two matrices contain all correct amplitude and phase information of the transmitted field.

For secure acoustic holography, an $N \times N$ random-phase matrix is first generated, where every phase element, $\phi_{i,j}^R$, within the matrix is randomly generated and obeys the uniform distribution (i.e., $\phi_{i,j}^R \sim [0, 2\pi]$). This random-phase matrix is the stochastic code containing the coding information and must be kept confidential. The hologram containing all correct information of the transmitted field will be then enciphered into an encoded hologram based on the random-phase matrix. The coding rules are that the amplitude information on the encoded hologram, $A_{i,j}^E$, remains unchanged, i.e.,

$$A_{i,j}^E = A_{i,j}; \quad (1)$$

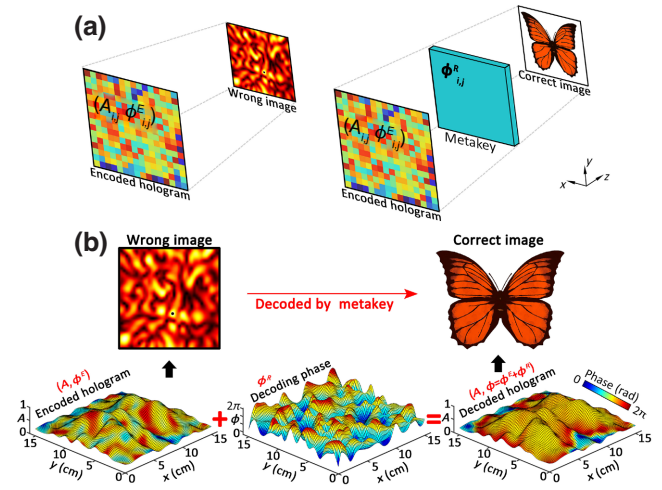


FIG. 1. Illustration of secure acoustic holography. (a) Encoded hologram contains the secure amplitude and enciphered phase information of the transmitted acoustic field, and an unreadable acoustic field will be generated directly using the encoded hologram (left panel). Acoustic metakey contains the decoding phase, and the desired field can be recovered with the aid of the metakey. (b) Encoded hologram, decoding phase provided by the metakey, and decoded hologram for the acoustic field of a butterfly.

however, the encoded phase information, $\phi_{i,j}^E$, is modulated as

$$\phi_{i,j}^E = \phi_{i,j} - \phi_{i,j}^R. \quad (2)$$

As a result, only an unreadable acoustic image (characterized by the acoustic field) can be obtained if directly using the encoded hologram [left panel in Fig. 1(a)].

To obtain the desired image, the encoded hologram has to be deciphered first. Here, we design an acoustic decoding metakey, such that it provides exactly the same additional phase as the precreated random matrix, i.e., $\phi_{i,j}^R$. Consequently, the acoustic waves generated by the encoded hologram will propagate through the acoustic metakey, and the additional phase information provided by the metakey will be added to the original encoded information. Finally, the desired image can be obtained based on the decoded hologram [right panel in Fig. 1(a)].

Details of the computation of acoustic holograms are shown below. A holographic pattern is first characterized by the acoustic pressure field, $P(x, y, z)$, where only the amplitude field is taken into consideration and the phase distribution is kept uniform. The field is then discretized into a collection of pixels, $P_m(x_m, y_m, z_m) = A_m(x_m, y_m, z_m)$, where m denotes the pixel number and the uniform phase is chosen to be zero. Hence, complex acoustic pressure information on the hologram, $p_{i,j} = A_{i,j} e^{\phi_{i,j}}$, can be obtained

based on the time-reversal method [7]:

$$p_{i,j} = A_{i,j} e^{\phi_{i,j}} = \sum_{m=1}^M \frac{A_m}{r_m} \exp(ikr_m), \quad (3)$$

where $k = 2\pi f / c$ is the wave number; $c = 343 \text{ m s}^{-1}$ is the sound speed of the background medium, air. M is the total number of image pixels, and r_m is the spatial distance between the image pixel and hologram pixel, i.e., $r_m^2 = (x_{i,j} - x_m)^2 + (y_{i,j} - y_m)^2 + (z_{i,j} - z_m)^2$.

Inversely, the acoustic field on the image plane can be also calculated analytically based on information contained in the hologram, i.e.,

$$P_m = \sum_{i,j=1}^N \frac{A_{i,j}}{r_{i,j}} \exp[-i(kr_{i,j} - \phi_{i,j})], \quad (4)$$

where $N \times N$ is the total number of hologram pixels, and the distance $r_{i,j}$ between spatial point (x, y, z) and hologram pixel $(x_{i,j}, y_{i,j}, z_{i,j})$ is calculated by $r_{i,j}^2 = (x - x_{i,j})^2 + (y - y_{i,j})^2 + (z - z_{i,j})^2$.

III. DESIGN OF ACOUSTIC METAKEY

The acoustic metakey is composed of a series of three-dimensional unit cells made of solid materials, as shown in Fig. 2(a). Each unit cell consists of a straight channel decorated with a series of panels. The size of each unit cell is chosen to be $10 \times 10 \times 10 \text{ mm}^3$. The wall thickness of the structure is $w = 0.5 \text{ mm}$, and the opening size of the panels, d , is adjusted to control the transmitted

phase shift of acoustic waves (for similar structures, see Refs. [54–56]).

Numerical results of the phase shift and the corresponding transmission rate, $|p_t/p_i|$, of the transmitted sound field through the unit cell are shown in Fig. 2(b), where p_i and p_t are the incident and transmitted acoustic pressures, respectively. From the results, the transmitted phase shift (black solid line) can cover the span of 2π when varying the geometry parameter, d/D , while keeping the transmission rate (red dots) at a high level.

Here, numerical simulations are conducted on a server (equipped with the AMD Ryzen Threadripper 3970X 32-core processor with 128 gigabytes of memory) using the “acoustic thermoviscous acoustic interaction, frequency domain” module in COMSOL Multiphysics, which is commercial software based on the finite-element method [see Fig. 2(b), inset]. Perfectly matched layers (PMLs) are used for the outer boundaries of the computation domain to prevent undesired reflections. A free tetrahedral mesh with a maximum size of $\lambda/5$ is used within the main computation domain, and a mapped mesh of eight layers is used for the perfectly matched layers. In particular, a finer mesh is configured near boundary layers to obtain acoustic fields precisely. The walls of the acoustic structure are set as sound-hard boundaries. The background pressure field is used with a working frequency of 40 kHz, which is the same as the operating frequency of the speaker array. The mass density and the sound speed of the background medium air are set as $\rho_0 = 1.21 \text{ kg m}^{-3}$ and $c_0 = 343 \text{ m s}^{-1}$, respectively. The transmitted phase shift of acoustic waves is obtained by the average sound pressure on the transmitted plane (boundary probe in the simulation setup).

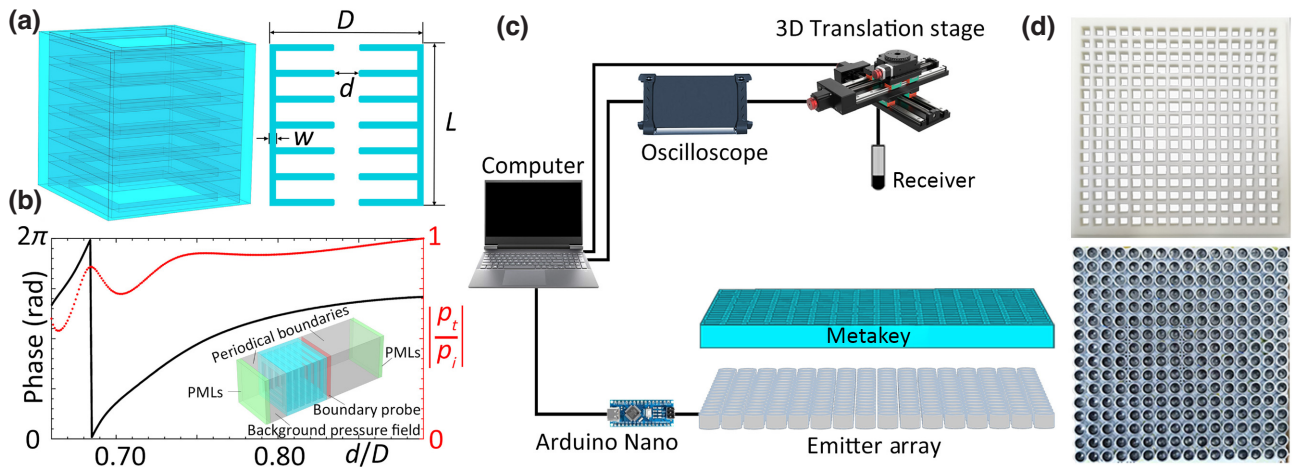


FIG. 2. Illustration of the acoustic metakey and experiment setup for measurements of acoustic fields. (a) Three-dimensional illustration and corresponding two-dimensional cross section of an element of the metakey. (b) Phase shift and transmission rate of the sound field when varying the geometric parameter of the element. Inset, simulation setup for the unit of the acoustic metakey. (c) Emitter array consisting of 16×16 elements is connected to a computer through an Arduino Nano board. Ultrasonic receiver is mounted on a translation stage, which is directly controlled by the computer through a MATLAB script. Received signals are captured by the oscilloscope and then transmitted to the computer. (d) Photos of a metakey sample and the emitter array.

The experiments are carried out in three-dimensional space with the illustration shown in Fig. 2(c). A speaker array consisting of 16×16 air-coupled ultrasonic transducers of 1 cm in diameter (Murata MA40S4S, driven by a 12-V peak-to-peak square-wave signal and producing a sinusoidal output at 40 kHz) is used as the source, and another air-coupled ultrasonic transducer (Murata MA40S4S) is placed at a distance of 15 cm behind the sample of acoustic metakeys as a receiver. The receiver is connected to a translation stage, which directly communicates with a laptop through a MATLAB script. The scanning area at the image plane is $15.4 \times 15.4 \text{ cm}^2$ with a scanning resolution of 2 mm. Data from the receiver is collected via the oscilloscope (PicoScope 54444D) at the laptop for further operations. Enlarged photos of the speaker array and the metakey are shown in Fig. 2(d). The metakey containing decoding information is designed based on the random-phase matrix [57]. Here, all samples are made of photosensitive resin and are manufactured via the three-dimensional printing technique (Lite600HD, 0.1 mm in precision). Each metakey consists of 16×16 unit cells with a sample size of $16 \times 16 \times 1 \text{ cm}^3$.

IV. SECURE ACOUSTIC HOLOGRAPHY

A. Holographic image of a butterfly

To demonstrate the secure acoustic hologram proposed here, a holographic image of a butterfly, as shown in Fig. 3(a), is first chosen as an example. The amplitude and phase information on the encoded hologram are calculated based on Eqs. (1)–(3), as shown in Figs. 3(b) and 3(c), and the random-phase matrix is generated, with the results shown in Fig. 3(d). Here, N is chosen to be 16, and the distance between the image plane and the hologram plane is 15 cm, i.e., $z_m = 15 \text{ cm}$ and $z_{i,j} = 0 \text{ cm}$. The source

employed in our experiments is a speaker array consisting of 16×16 air-coupled ultrasonic transducers, where the initial amplitude and phase of each speaker can be adjusted individually, so that both the amplitude and phase information on the encoded hologram can be directly achieved by the speaker array. Another air-coupled ultrasonic transducer is placed at a spatial distance of 15 cm away from the hologram to receive transmitted signals. The acoustic field directly generated by the encoded hologram is shown in Fig. 3(e), where an unreadable image is obtained as expected.

To access the desired image, the information contained within the encoded hologram must be deciphered first. Hence, here an acoustic metakey possessing the confidential stochastic code, i.e., the previous random-phase profile [Fig. 3(d)], is designed and placed in front of the speaker array. The acoustic waves generated by the encoded hologram will pass through the metakey, and the enciphered information is then decoded and deciphered.

Figures 3(f)–3(h) present the acoustic intensity distribution on the image plane for the analytical results based on Eq. (4), the numerical simulation based on the finite-element method, and the experimental measurements, respectively. From the results, the predesigned pattern of a butterfly is clearly observed after being deciphered by the metakey, proving the excellent performance of the secure acoustic holography proposed here and validating the ability of the metakey to generate high-quality acoustic holograms.

B. Holographic image of sunglasses

To demonstrate the flexibility of the proposed secure acoustic hologram, a holographic image of sunglasses is presented here [Fig. 4(a)]. Similarly, the amplitude and

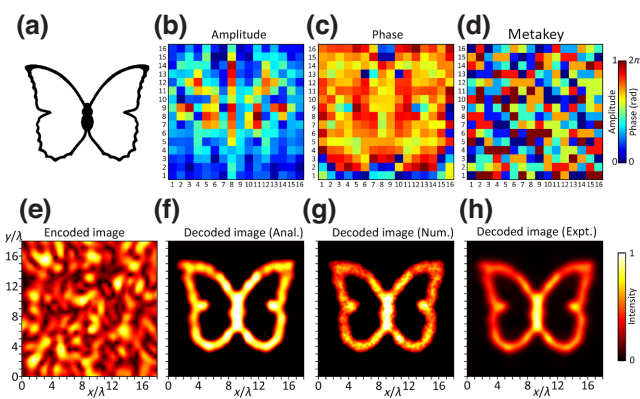


FIG. 3. Results for the field of a butterfly. (a) Desired field of a butterfly. (b) Encoded amplitude and (c) phase information for the desired field. (d) Additional phase provided by the metakey. (e) Unreadable field generated directly by the encoded hologram. (f) Analytical, (g) numerical, and (h) experimental results for the field generated by the decoded hologram.

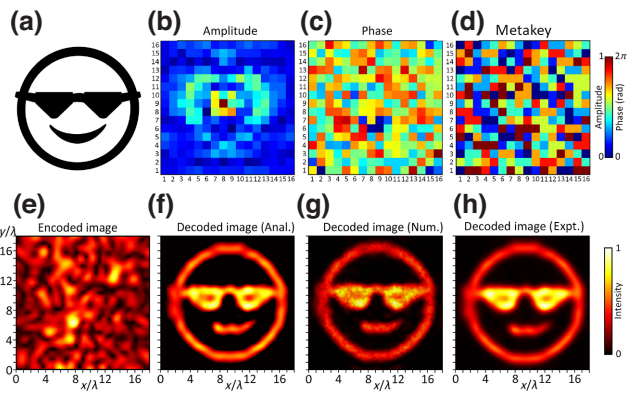


FIG. 4. Results for the field of sunglasses. (a) Desired field of sunglasses. (b) Encoded amplitude and (c) phase information for the desired field. (d) Additional phase provided by the metakey. (e) Unreadable field generated directly by the encoded hologram. (f) Analytical, (g) numerical, and (h) experimental results for the field generated by the decoded hologram.

phase information on the encoded hologram are calculated based on Eqs. (1)–(3), with the results shown in Figs. 4(b) and 4(c). The random-phase matrix containing the coding information is shown in Fig. 4(d), which is the same as that in Fig. 3(d). Here, as long as the random-phase matrix (i.e., the stochastic code) is still secure and confidential, it can be kept unchanged. Otherwise, a new random matrix must be regenerated to keep the information secret.

The acoustic field directly generated by the encoded hologram is shown in Fig. 4(e), where an unreadable image is again obtained as expected. Then, the previous metakey possessing the same stochastic code is placed in front of the speaker array to decode the enciphered information contained in the encoded hologram.

Figures 4(f)–4(h) exhibit the acoustic intensity distribution on the image plane for the analytical results [Eq. (4)], the numerical simulation, and the experimental measurements, respectively. From the results, the predesigned pattern of sunglasses is clearly observable, proving the high fidelity and confidentiality of the secure acoustic holography proposed here.

C. Holographic image of the letters NJUST

To further demonstrate the flexibility of the secure acoustic hologram proposed, a holographic image of the letters NJUST is presented here [Fig. 5(a)], where multiple letters are transmitted on a single holographic image. Similarly, the amplitude and phase information on the encoded hologram are calculated based on Eqs. (1)–(3), with the results shown in Figs. 5(b) and 5(c). The random-phase matrix containing the coding information is shown in Fig. 5(d).

The acoustic field directly generated by the encoded hologram is shown in Fig. 5(e), where an unreadable image

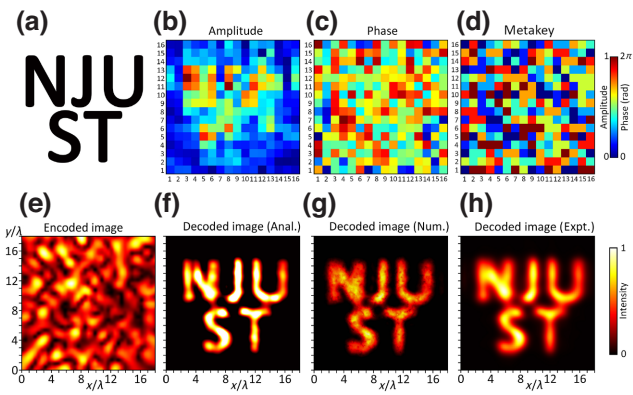


FIG. 5. Results for the field of letters NJUST. (a) Desired field of NJUST. (b) Encoded amplitude and (c) phase information for the desired field. (d) Additional phase provided by the metakey. (e) Unreadable field generated directly by the encoded hologram. (f) Analytical, (g) numerical, and (h) experimental results for the field generated by the decoded hologram.

is again obtained as expected. Then, the previous metakey possessing the same stochastic code is placed in front of the speaker array to decode the enciphered information contained in the encoded hologram. Figures 5(f)–5(h) show the acoustic intensity distribution on the image plane for the analytical results [Eq. (4)], the numerical simulation, and the experimental measurements, respectively. From the results, the predesigned pattern of the letters NJUST is well recovered and clearly observed.

V. VULNERABILITY TEST OF THE METAKEY

We have experimentally shown that different metaholograms can be realized using the same metakey (see Figs. 3–5), and the transmitted information can be protected when the metakey is mistakenly accessed by others. To examine the security and reliability of the metakey, the vulnerability of the proposed concept of secure acoustic holography has been tested when a whole part of the metakey is accessed by others (Fig. 6). The match ratio between the metaholographic images using the partial metakey and the entire metakey is shown in Fig. 6(a), where the match ratio decreases with the area of the partial metakey characterized by n [the deciphered part of the metakey is marked by shading in the inset of Fig. 6(a)]. The reconstructed image becomes fuzzy, even when a major part of the metakey is used [$n = 15$; see Fig. 6(b)], and the image of sunglasses is hard to identify when n is reduced to 12. Here, the match ratio is obtained by $(1 - e) \times 100\%$, where e represents the normalized root-mean-square error of the image reconstructed using a partial metakey, and the match ratio reaches 100% when using the whole metakey. Therefore, the framework of secure acoustic holography proposed here exhibits a pretty good security performance, even though almost the simplest encryption method is used for the decoding metakey.

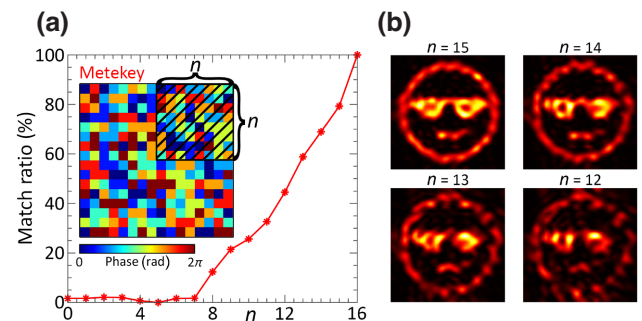


FIG. 6. Vulnerability test of the metakey. (a) Match ratio between holographic images using the partial metakey and the entire metakey. Inset, partial metakey (marked by the shading) containing $n \times n$ effective phases. (b) Intensity fields using partial metakeys with different n .

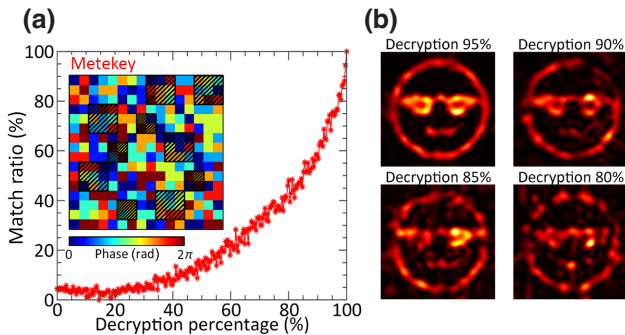
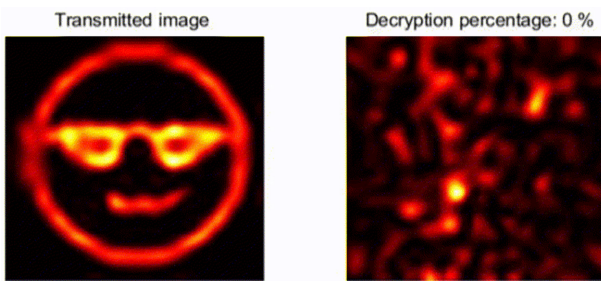


FIG. 7. Vulnerability test of the metakey when the information at random locations is deciphered. (a) Match ratio between the holographic images using the partial metakey and the entire metakey. Inset, partially deciphered metakey is illustrated by shading. (b) Intensity fields using partially deciphered metakeys.

To further test the security of the system, another situation, when the specific information at some of its random locations is deciphered, is considered (Fig. 7). The deciphered parts of the metakey are illustrated by shading in the inset in Fig. 7(a), where the area ratio between the deciphered part and the whole metakey is characterized by the decryption percentage. The match ratio between metaholographic images obtained using the partial metakey and the entire metakey is shown in Fig. 7(a), where the match ratio increases with the decryption percentage. The reconstructed image is still fuzzy even when 85% of the metakey is deciphered [Fig. 7(b)], and the image is barely recognized when the decryption percentage reaches 90%, which again confirms the security and reliability of the secure acoustic holography proposed here; see Video 1 for the dynamic evolution of the reconstructed holographic images when the information of the metakey is deciphered [57].

We have also examined the effect of the image location on the quality of the reconstructed hologram. Figure 8 shows reconstructed images at different spatial locations in the z direction. The metaholographic image becomes blurry when the deviation of the image plane from the preset location is larger than 2λ . This spatial location of the



VIDEO 1. Dynamic evolution of reconstructed holographic images when the information of the metakey is deciphered.

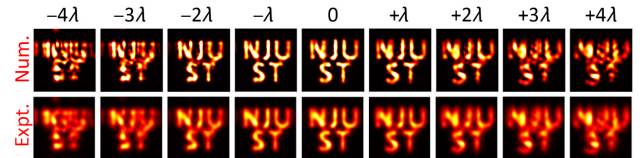


FIG. 8. Experimental and analytical results for NJUST at different positions in the z direction. Corresponding values above images indicate the distance between the image plane and the predesigned location.

image plane provides us with another degree of freedom for information encryption in addition to the transmitted encrypted amplitude and phase information and the secure metakey [57].

VI. CONCLUSION

We have proposed and investigated a framework for secure acoustic holography. The latter is achieved via an encoded hologram decoded by a transmissive acoustic metakey. An acoustic speaker array consisting of 16×16 air-coupled ultrasonic transducers has been used to generate the encoded hologram containing both amplitude and enciphered phase information. An unreadable image is received if directly using the encoded hologram, and the desired image can be obtained only with the aid of the correctly decoding metakey. An alternative class of unit cells that could effectively modulate transmitted phase shifts of acoustic waves was designed and used to build the acoustic metakey, which could decode the enciphered information and recover the predesigned images with high fidelity. As a proof of concept, we analytically, numerically, and experimentally demonstrated secure acoustic holography for the patterns of a butterfly, sunglasses, and the letters NJUST. The results exhibit a pretty good security performance, even when a major part of the metakey is deciphered. Our work provides a framework for secure acoustic communication with the advantages of simple design, flexible functionality, and high quality of reconstructed images. The results could be beneficial for a variety of acoustic applications involving secure communications and underwater communications, where optical and electromagnetic counterparts may not be the first option.

For the secure acoustic holography proposed here, the fixed metakey can be recycled, as long as the random-phase information contained in the metakey is still secure and confidential. Since the simple encryption strategy of random-phase distortion is used here, there is still a chance for the proposed method to be potentially deciphered using some optimization methods, for example, phase-retrieval methods under a certain amount of iterations [58]. However, more complex encryption strategies of the metakey could be easily extended based on the framework proposed here. In addition, metakey capable of both amplitude and

phase modulations can be considered to further improve the security of the system.

ACKNOWLEDGMENTS

This work is supported by the National Natural Science Foundation of China (Grant No. 12204241), the Natural Science Foundation of Jiangsu Province (Grant No. BK20220924), and the Fundamental Research Funds for the Central Universities (Grants No. 30923011019 and No. 020414380195).

- [1] Kai Melde, Andrew G. Mark, Tian Qiu, and Peer Fischer, Holograms for acoustics, *Nature* **537**, 518 (2016).
- [2] Yangbo Xie, Chen Shen, Wenqi Wang, Junfei Li, Dingjie Suo, Bogdan-Ioan Popa, Yun Jing, and Steven A. Cummer, Acoustic holographic rendering with two-dimensional metamaterial-based passive phased array, *Sci. Rep.* **6**, 35437 (2016).
- [3] Asier Marzo, Sue Ann Seah, Bruce W. Drinkwater, Deepak Ranjan Sahoo, Benjamin Long, and Sriram Subramanian, Holographic acoustic elements for manipulation of levitated objects, *Nat. Commun.* **6**, 1 (2015).
- [4] Asier Marzo and Bruce W. Drinkwater, Holographic acoustic tweezers, *Proc. Natl. Acad. Sci.* **116**, 84 (2019).
- [5] Ryuji Hirayama, Diego Martinez Plasencia, Nobuyuki Masuda, and Sriram Subramanian, A volumetric display for visual, tactile and audio presentation using acoustic trapping, *Nature* **575**, 320 (2019).
- [6] Ye Tian, Qi Wei, Ying Cheng, and Xiaojun Liu, Acoustic holography based on composite metasurface with decoupled modulation of phase and amplitude, *Appl. Phys. Lett.* **110**, 191901 (2017).
- [7] Yifan Zhu, Jie Hu, Xudong Fan, Jing Yang, Bin Liang, Xuefeng Zhu, and Jianchun Cheng, Fine manipulation of sound via lossy metamaterials with independent and arbitrary reflection amplitude and phase, *Nat. Commun.* **9**, 1 (2018).
- [8] Shi-Wang Fan, Yifan Zhu, Liyun Cao, Yan-Feng Wang, A-Li Chen, Aurélien Merkel, Yue-Sheng Wang, and Badreddine Assouar, Broadband tunable lossy metasurface with independent amplitude and phase modulations for acoustic holography, *Smart Mater. Struct.* **29**, 105038 (2020).
- [9] Mingxin Xu, William S. Harley, Zhichao Ma, Peter V.S. Lee, and David J. Collins, Sound-speed modifying acoustic metasurfaces for acoustic holography, *Adv. Mater.* **34**, 2208002 (2023).
- [10] Shubhi Bansal, Christabel Choi, James Hardwick, Biswajoy Bagchi, Manish K. Tiwari, and Sriram Subramanian, Transmissive labyrinthine acoustic metamaterial-based holography for extraordinary energy harvesting, *Adv. Eng. Mater.* **25**, 2201117 (2022).
- [11] Jin Zhang, Ye Tian, Ying Cheng, and Xiaojun Liu, Acoustic holography using composite metasurfaces, *Appl. Phys. Lett.* **116**, 030501 (2020).
- [12] Jinwook Kim, Sandeep Kasoji, Phillip G. Durham, and Paul A. Dayton, Acoustic holograms for directing arbitrary cavitation patterns, *Appl. Phys. Lett.* **118**, 051902 (2021).
- [13] Sergio Jiménez-Gambín, Noé Jiménez, Antonios N. Pouliopoulos, José M. Benlloch, Elisa E. Konofagou, and Francisco Camarena, Acoustic holograms for bilateral blood-brain barrier opening in a mouse model, *IEEE Trans. Biomed. Eng.* **69**, 1359 (2021).
- [14] Sergio Jiménez-Gambín, Noé Jiménez, José María Benlloch, and Francisco Camarena, Holograms to focus arbitrary ultrasonic fields through the skull, *Phys. Rev. Appl.* **12**, 014016 (2019).
- [15] Zhichao Ma, Andrew W. Holle, Kai Melde, Tian Qiu, Korbinian Poeppel, Vincent Mauricio Kadiri, and Peer Fischer, Acoustic holographic cell patterning in a biocompatible hydrogel, *Adv. Mater.* **32**, 1904181 (2020).
- [16] Zhichao Ma, Hyungmok Joh, Donglei Emma Fan, and Peer Fischer, Dynamic ultrasound projector controlled by light, *Adv. Sci.* **9**, 2104401 (2022).
- [17] Zhichao Ma, Kai Melde, Athanasios G. Athanassiadis, Michael Schau, Harald Richter, Tian Qiu, and Peer Fischer, Spatial ultrasound modulation by digitally controlling microbubble arrays, *Nat. Commun.* **11**, 4537 (2020).
- [18] Yangbo Xie, Chen Shen, Wenqi Wang, Junfei Li, Dingjie Suo, Bogdan-Ioan Popa, Yun Jing, and Steven A. Cummer, Acoustic holographic rendering with two-dimensional metamaterial-based passive phased array, *Sci. Rep.* **6**, 1 (2016).
- [19] Michael D. Brown, Phase and amplitude modulation with acoustic holograms, *Appl. Phys. Lett.* **115**, 053701 (2019).
- [20] Chuanxin Zhang, Xue Jiang, Shuai Han, Jiajie He, Yan Zheng, Boyi Li, and Dean Ta, Converged wireless infrastructure with acoustic holographic array, *Appl. Phys. Rev.* **9**, 041413 (2022).
- [21] Yifan Zhu and Badreddine Assouar, Systematic design of multiplexed-acoustic-metasurface hologram with simultaneous amplitude and phase modulations, *Phys. Rev. Mater.* **3**, 045201 (2019).
- [22] Haider Butt, Yunuen Montelongo, Tim Butler, Ranjith Rajesekharan, Qing Dai, Sai G. Shiva-Reddy, Timothy D. Wilkinson, and Gehan A. J. Amarasinghe, Carbon nanotube based high resolution holograms, *Adv. Mater.* **24**, OP331 (2012).
- [23] Stephane Larouche, Yu-Ju Tsai, Talmage Tyler, Nan M. Jokerst, and David R. Smith, Infrared metasurface phase holograms, *Nat. Mater.* **11**, 450 (2012).
- [24] Benny Walther, Christian Helgert, Carsten Rockstuhl, Frank Setzpfandt, Falk Eilenberger, Ernst-Bernhard Kley, Falk Lederer, Andreas Tuennermann, Thomas Pertsch, *et al.*, Spatial and spectral light shaping with metamaterials, *Adv. Mater.* **24**, 6300 (2012).
- [25] Xingjie Ni, and Alexander V. Kildishev, and Vladimir M. Shalaev, Metasurface holograms for visible light, *Nat. Commun.* **4**, 2807 (2013).
- [26] Lingling Huang, Xianzhong Chen, Holger Mühlenbernd, Hao Zhang, Shumei Chen, Benfeng Bai, Qiaofeng Tan, Guofan Jin, Kok-Wai Cheah, Cheng-Wei Qiu, *et al.*, Three-dimensional optical holography using a plasmonic metasurface, *Nat. Commun.* **4**, 2808 (2013).
- [27] Guoxing Zheng, Holger Mühlenbernd, Mitchell Kenney, Guixin Li, Thomas Zentgraf, and Shuang Zhang, Metasurface holograms reaching 80% efficiency, *Nat. Nanotechnol.* **10**, 308 (2015).

- [28] Dandan Wen, Fuyong Yue, Guixin Li, Guoxing Zheng, Kinlong Chan, Shumei Chen, Ming Chen, King Fai Li, Polis Wing Han Wong, Kok Wai Cheah, Edwin Yue Bun Pun, Shuang Zhang, and Xianzhong Chen, Helicity multiplexed broadband metasurface holograms, *Nat. Commun.* **6**, 8241 (2015).
- [29] Lingling Huang, Holger Muhlenbernd, Xiaowei Li, Xu Song, Benfeng Bai, Yongtian Wang, and Thomas Zentgraf, Broadband hybrid holographic multiplexing with geometric metasurfaces, *Adv. Mater.* **27**, 6444+ (2015).
- [30] Lei Wang, Sergey Kruk, Hanzhi Tang, Tao Li, Ivan Kravchenko, Dragomir N. Neshev, and Yuri S. Kivshar, Grayscale transparent metasurface holograms, *Optica* **3**, 1504 (2016).
- [31] Wenyu Zhao, Bingyi Liu, Huan Jiang, Jie Song, Yanbo Pei, and Yongyuan Jiang, Full-color hologram using spatial multiplexing of dielectric metasurface, *Opt. Lett.* **41**, 147 (2016).
- [32] Bo Wang, Fengliang Dong, Qi-Tong Li, Dong Yang, Chenwei Sun, Jianjun Chen, Zhiwei Song, Lihua Xu, Weiguo Chu, Yun-Feng Xiao, Qihuang Gong, and Yan Li, Visible-frequency dielectric metasurfaces for multiwavelength achromatic and highly dispersive holograms, *Nano. Lett.* **16**, 5235 (2016).
- [33] Qiu Wang, Xueqian Zhang, Yuehong Xu, Jianqiang Gu, Yanfeng Li, Zhen Tian, Ranjan Singh, Shuang Zhang, Jiaguang Han, and Weili Zhang, Broadband metasurface holograms: Toward complete phase and amplitude engineering, *Sci. Rep.* **6**, 32867 (2016).
- [34] Adam C. Overvig, Sajan Shrestha, Stephanie C. Malek, Ming Lu, Aaron Stein, Changxi Zheng, and Nanfang Yu, Dielectric metasurfaces for complete and independent control of the optical amplitude and phase, *Light Sci. Appl.* **8**, 92 (2019).
- [35] Chengjun Zou, Andrei Komar, Stefan Fasold, Justus Bohn, Alexander A. Muravsky, Anatoli A. Murauski, Thomas Pertsch, Dragomir N. Neshev, and Isabelle Staude, Electrically tunable transparent displays for visible light based on dielectric metasurfaces, *ACS Photonics* **6**, 1533 (2019).
- [36] Xingbo Liu, Qiu Wang, Xueqian Zhang, Hua Li, Quan Xu, Yuehong Xu, Xieyu Chen, Shaonian Li, Meng Liu, Zhen Tian, Caihong Zhang, Chongwen Zou, Jiaguang Han, and Weili Zhang, Thermally dependent dynamic metaholography using a vanadium dioxide integrated metasurface, *Adv. Opt. Mater.* **7**, 1900175 (2019).
- [37] Jianxiong Li, Simon Kamin, Guoxing Zheng, Frank Neubrech, Shuang Zhang, and Na Liu, Addressable metasurfaces for dynamic holography and optical information encryption, *Sci. Adv.* **4**, eaar6768 (2018).
- [38] Stephanie C. Malek, Ho-Seok Ee, and Ritesh Agarwal, Strain multiplexed metasurface holograms on a stretchable substrate, *Nano. Lett.* **17**, 3641 (2017).
- [39] Peixia Zheng, Qi Dai, Zile Li, Zhiyuan Ye, Jun Xiong, Hong-Chao Liu, Guoxing Zheng, and Shuang Zhang, Metasurface-based key for computational imaging encryption, *Sci. Adv.* **7**, eabg0363 (2021).
- [40] Lei Jin, Yao-Wei Huang, Zhongwei Jin, Robert C. Devlin, Zhaogang Dong, Shengtao Mei, Menghua Jiang, Wei Ting Chen, Zhun Wei, Hong Liu, Jinghua Teng, Aaron Danner, Xiangping Li, Shumin Xiao, Shuang Zhang, Changyuan Yu, Joel K. W. Yang, Federico Capasso, and Cheng-Wei Qiu, Dielectric multi-momentum meta-transformer in the visible, *Nat. Commun.* **10**, 4789 (2019).
- [41] Inki Kim, Heonyeong Jeong, Joohoon Kim, Younghwan Yang, Dasol Lee, Trevon Badloe, Gyeongtae Kim, and Junsuk Rho, Dual-band operating metaholograms with heterogeneous meta-atoms in the visible and near-infrared, *Adv. Opt. Mater.* **9**, 2100609 (2021).
- [42] Seyedeh Mahsa Kamali, Ehsan Arbabi, Amir Arbabi, Yu Horie, MohammadSadegh Faraji-Dana, and Andrei Faraon, Angle-multiplexed metasurfaces: Encoding independent wavefronts in a single metasurface under different illumination angles, *Phys. Rev. X* **7**, 041056 (2017).
- [43] Hui Gao, Yuxi Wang, Xuhao Fan, Bin Zhang Jiao, Ting-gan Li, Chenglin Shang, Cheng Zeng, Leimin Deng, Wei Xiong, Jinsong Xia, and Minghui Hong, Dynamic 3D metaholography in visible range with large frame number and high frame rate, *Sci. Adv.* **6**, eaba8595 (2020).
- [44] Jaekyung Kim, Junhwa Seong, Younghwan Yang, Seong-Won Moon, Trevon Badloe, and Junsuk Rho, Tunable metasurfaces towards versatile metalenses and metaholograms: A review, *Adv. Photonics* **4**, 024001 (2022).
- [45] Jaehyuck Jang, Heonyeong Jeong, Guangwei Hu, Cheng-Wei Qiu, Ki Tae Nam, and Junsuk Rho, Kerker-conditioned dynamic cryptographic nanoprints, *Adv. Opt. Mater.* **7**, 1801070 (2019).
- [46] Inki Kim, Jaehyuck Jang, Gyeongtae Kim, Jihae Lee, Trevon Badloe, Jungho Mun, and Junsuk Rho, Pixelated bifunctional metasurface-driven dynamic vectorial holographic color prints for photonic security platform, *Nat. Commun.* **12**, 3614 (2021).
- [47] Peixia Zheng, Qi Dai, Zile Li, Zhiyuan Ye, Jun Xiong, Hong-Chao Liu, Guoxing Zheng, and Shuang Zhang, Metasurface-based key for computational imaging encryption, *Sci. Adv.* **7**, eabg0363 (2021).
- [48] Kevin T. P. Lim, Hailong Liu, Yeqing Liu, and Joel K. W. Yang, Holographic colour prints for enhanced optical security by combined phase and amplitude control, *Nat. Commun.* **10**, 25 (2019).
- [49] Yanjun Bao, Ying Yu, Haofei Xu, Chao Guo, Juntao Li, Shang Sun, Zhang-Kai Zhou, Cheng-Wei Qiu, and Xue-Hua Wang, Full-colour nanoprint-hologram synchronous metasurface with arbitrary hue-saturation-brightness control, *Light Sci. Appl.* **8**, 95 (2019).
- [50] Bogdan-Ioan Popa, Lucian Zigoneanu, and Steven A. Cummer, Experimental acoustic ground cloak in air, *Phys. Rev. Lett.* **106**, 253901 (2011).
- [51] Xu-Dong Fan, Bin Liang, Jing Yang, and Jian-Chun Cheng, Illusion for airborne sound source by a closed layer with subwavelength thickness, *Sci. Rep.* **9**, 1750 (2019).
- [52] Yifan Zhu, Xudong Fan, Bin Liang, Jianchun Cheng, and Yun Jing, Ultrathin acoustic metasurface-based schroeder diffuser, *Phys. Rev. X* **7**, 021034 (2017).
- [53] Xudong Fan, Yifan Zhu, Zihao Su, Ning Li, Xiaolong Huang, Yang Kang, Can Li, Chunsheng Weng, Hui Zhang, Weiwei Kan, *et al.*, Transverse particle trapping using finite bessel beams based on acoustic metamaterials, *Phys. Rev. Appl.* **19**, 034032 (2023).

- [54] Xudong Fan, Yifan Zhu, Zihao Su, Ning Li, Xiaolong Huang, Yang Kang, Can Li, Chunsheng Weng, Hui Zhang, Bin Liang, *et al.*, Ultrabroadband and reconfigurable transmissive acoustic metascreen, *Adv. Funct. Mater.* **33**, 2300752 (2023).
- [55] Yong Li, Xue Jiang, Bin Liang, Jian-chun Cheng, and Likun Zhang, Metascreen-based acoustic passive phased array, *Phys. Rev. Appl.* **4**, 024003 (2015).
- [56] Liping Ye, Chunyin Qiu, Jiuyang Lu, Kun Tang, Han Jia, Manzhu Ke, Shasha Peng, and Zhengyou Liu, Making sound vortices by metasurfaces, *AIP Adv.* **6**, 085007 (2016).
- [57] See the Supplemental Material at <http://link.aps.org-supplemental/10.1103/PhysRevApplied.20.044048> for detailed parameters of the metakey and vulnerability tests of the metakey under attack.
- [58] Byungjae Hwang, Taeseong Woo, Cheolwoo Ahn, and Jung-Hoon Park, Imaging through random media using coherent averaging, *Laser Photonics Rev.* **17**, 2200673 (2023).